Monocarboxylate transporter 4 promotes the migration of non-cancerous L929 fibroblast cells by activating the IGF1/IGF1R/PIK3R3/SGK1 axis

XIAOJU ZHOU[1], SHUO WANG[1], YANYAN LI[1], HE ZHAO[1], XUE HAN[1], YUE YU[1], YU CHEN[1], YU YANG[2], XIAONAN MA[2], HONGJING HUO[1,3], MANTING ZHANG[1,4], YONGSHAN ZHAO[2] and NINGNING MA[1]

[1]Wuya College of Innovation; [2]Department of Biochemistry and Molecular Biology, School of Life Science and Biopharmaceutics, Shenyang Pharmaceutical University, Shenyang, Liaoning 110016, P.R. China

Abstract. The tumor microenvironment (TME) and Warburg effect are critical for the regulation of tumor metastasis. The monocarboxylate transporter (MCT) family members, particularly MCT4, which is encoded by the solute carrier family 16 member 3 gene, play an important role in the regulation of the TME and mediation of the Warburg effect by transporting lactate out of cancer cells. Migration and invasion are two key features of metastasis. Few studies have investigated the mechanism by which MCT4 promotes cell migration, and the suggested mechanisms by which MCT4 promotes migration vary in different tumor cell models. The purpose of the present study was to use non-cancerous cells as a research model to investigate the specific mechanism underlying the promotion of migration by MCT4. In a previous study, murine L929 cells overexpressing human MCT4 (MCT4-L929 cells) were generated and MCT4 was demonstrated to promote the migration and invasion of these non-cancerous cells. In the present study, MCT4-L929 cells and control-L929 cells were used to investigate the potential pathways and mechanisms through which MCT4 promotes cell migration. RNA sequencing analysis revealed 872 differentially expressed genes, comprising 337 and 535 upregulated and downregulated genes, respectively, in the MCT4-L929 cells. Reverse transcription-quantitative analysis and western blotting revealed that MCT4 overexpression increased the transcription and protein levels of insulin-like growth factor 1 (IGF1). In a wound healing assay, the migration of exogenous mouse IGF1-treated control-L929 cells was similar to that of MCT4-L929 cells. Additionally, the inhibition of IGF1 receptor (IGF1R) or serum/glucocorticoid regulated kinase 1 (SGK1), a downstream protein in the IGF1 and phosphoinositide 3-kinase PI3K regulatory subunit 3 (PIK3R3) pathways, in MCT4-L929 cells mitigated the cell migration-promoting effect of MCT4. These novel findings suggest that MCT4 may promote the migration of L929 fibroblast cells via activation of the IGF1/IGF1R/PIK3R3/SGK1 axis.

Introduction

Metastasis is responsible for the high mortality rate of patients with cancer (1). Cancer cell migration and invasion are important steps in tumor metastasis, which is a multistage process (2). Elucidation of the mechanisms underlying cell migration and invasion will provide improved understanding of the dynamics and complexity of tumor metastasis and facilitate the development of novel clinical interventions for patients with cancer (3).

Several studies have examined the proteins and regulatory mechanisms involved in cell migration and invasion. For example, heat shock factor 1 has been demonstrated to be involved in the migration and invasion of human melanoma cells (4). In addition, it has been reported that activated prostaglandin-endoperoxidase synthase 2/prostaglandin E2 contributes to the migration and invasion of U87 human glioblastoma cells (5), while tumor necrosis factor superfamily member 10 promotes the migration and invasion of cholangiocarcinoma cells (6). Thus, diverse proteins or mechanisms are involved in cell migration. However, studies on these proteins or pathways are limited only to certain types of tumors.

Previous studies have revealed that the tumor microenvironment (TME) plays a crucial role in the regulation of

Correspondence to: Professor Yongshan Zhao, Department of Biochemistry and Molecular Biology, School of Life Science and Biopharmaceutics, Shenyang Pharmaceutical University, 103 Wenhua Road, Shenyang, Liaoning 110016, P.R. China
E-mail: zhao09081@163.com

Professor Ningning Ma, Wuya College of Innovation, Shenyang Pharmaceutical University, 103 Wenhua Road, Shenyang, Liaoning 110016, P.R. China
E-mail: maningning@syphu.edu.cn

Present addresses: [3]Department of Biological Drug Discovery, Simcere Pharmaceutical Group, Shanghai 201321; [4]Biopharmaceutical Department II, Shanghai Hengrui Pharmaceuticals Co., Ltd., Shanghai 200245, P.R. China

metastasis (7). The association between cancer cell metabolism and metastasis has piqued the interest of the scientific community (8). Metabolic reprogramming, which is a hallmark of cancer metastasis, involves a global metabolic shift toward increased glycolysis, known as the Warburg effect, to meet the energy demands of tumor cells and the TME (9). The Warburg effect is reported to promote tumor metastasis. Metastatic cancer cells experience increased oxidative stress, and the Warburg effect helps to reduce the oxidative stress in cancer cells via the inhibition of mitochondrial oxidative metabolism, thereby promoting the spread of metastases. Furthermore, the acidified TME, which develops due to the secretion of lactate from the cancer cells, increases the migratory and invasive activity of the cancer cells (10).

Most cancer cells rely on the Warburg effect for energy generation, which is accompanied by the production of increased quantities of lactate (11). Monocarboxylate transporter (MCT) family members, particularly MCT4, which is encoded by the solute carrier family 16 member 3 (*SLC16A3*) gene, are associated with lactate export from cells (12). The expression of MCT4 is upregulated in various tumor cells, including breast, lung, pancreatic, bladder cancer and colorectal cancer cells (13-17). Also, the upregulation of MCT4 expression is strongly associated with a poor prognosis in patients with cancer (15-17).

In previous studies the knockdown of MCT4 expression was shown to decrease the migration and invasion of lung cancer (18), oral squamous cell carcinoma (16), hepatocellular carcinoma (19), pancreatic ductal adenocarcinoma (20), prostate cancer (21), glioma (22) and breast cancer cells (23). These studies involved the transient silencing of MCT4 in various types of tumor cells and were mostly limited to describing the decreased migration after MCT4 silencing. Few studies have investigated the mechanism by which MCT4 promotes cell migration, and the mechanism by which MCT4 promotes migration has been found to vary, with inconsistency between different tumor cell models. In our previous study, human MCT4 was expressed in non-cancerous L929 cells via stable transfection and the overexpression of MCT4 was demonstrated to promote the migration and invasion of the non-cancerous L929 fibroblast cells (24). Notably, the homology of human and mouse MCT4 proteins is as high as 88%. The present study used transcriptomic sequencing and protein-protein interaction (PPI) analysis of these cells to identify key differentially expressed genes (DEGs) and key networks to elucidate the potential mechanisms by which MCT4 promotes cell migration.

Analysis of the DEGs indicated that insulin-like growth factor 1 (*Igf1*) was the most critical DEG. Therefore, the function of IGF1 in MCT4-overexpressing L929 cells was also investigated, and the potential mechanism by which MCT4 drives the migration of non-cancerous L929 fibroblast cells was identified.

Materials and methods

Cells and cell culture. L929 cells, which are non-cancerous murine cells that do not express MCT4, were obtained from the American Type Culture Collection (ATCC). L929 cell lines stably expressing human MCT4 were constructed as previously described (24). The human *SLC16A3* gene sequence and enhanced green fluorescent protein (EGFP) gene sequence were inserted into a pcDNA3.0 vector, and the plasmids were transfected into host L929 cells by electroporation. Three L929 cell lines with high MCT4 expression were selected (3E10, 4D11 and 8E4), and the transfected human MCT4 was confirmed to be active in the murine L929 cells. Additionally, three L929 cell lines expressing EGFP protein were chosen as control cell lines (C5, H9 and 2H6). These were generated using the same transfection and screening protocol as was used to generate the MCT4-overexpressing cells. In the following sections, L929 cells expressing MCT4 or EGFP are referred to as MCT4-L929 or control-L929 cells, respectively. The cells were cultured in CSC03-CL medium (cat. no. Y3020; Zhejiang Yishengke Biotechnology Co., Ltd.) supplemented with 10% fetal bovine serum (FBS; Gibco; Thermo Fisher Scientific, Inc.) and 600 μg/ml G418 (cat. no. G15000; Vazyme Biotech Co., Ltd.) at 37°C in an atmosphere containing 5% CO_2. Cell counts and viability were measured using an automated cell counter (Shanghai Ruiyu Biotech Co., Ltd.) with trypan blue staining (cat. no. 93595; Sigma-Aldrich; Merck KGaA).

RNA sequencing (RNA-seq). The three control-L929 cell lines (C5, H9 and 2H6) and three MCT4-L929 cell lines (3E10, 4D11 and 8E4) were subjected to RNA-seq using an Illumina platform. Total RNA was isolated using TRIzol (cat. no. 15596026, Invitrogen). Library preparation and sequencing were performed at Shanghai Personal Biotechnology Co, Ltd (Shanghai, China). The mixed library was diluted to 2 nM and then denatured by alkali to create a single-stranded library. The paired-end method was used with 150 base pairs for each end length. HISTAT2 (version 2.2.1, ccb.jhu.edu/software/hisat2/index.shtml) was used to map the reads to the Mus_musculus.GRCm38.dna.primary_assembly. fa.gz genome. The transcriptome coverage was in the range of 93.43-94.98%. The quality of the data is assessed based on factors including the Q20 ratio (the ratio of bases whose base recognition accuracy is over 99%), the Q30 ratio (the ratio of bases whose base recognition accuracy is over 99.9%), the Total_Mapped ratio (the ratio of total number of sequences of the reference genome on the alignment out of all clean reads), and Uniquely_Mapped ratio (the ratio of sequences aligned to only one position on the reference genome out of Total_Mapped). DEGs between the control-L929 and MCT4-L929 cells were identified based on the following criteria: |log$_2$ fold change (FC)|>1 and P<0.05.

Bioinformatics. Gene Ontology (GO: geneontology.org/) and Kyoto Encyclopedia of Genes and Genomes (KEGG: http://www.kegg.jp/kegg) enrichment analyses were performed. The degree of enrichment was evaluated based on the rich factor, the false discovery rate (FDR) and the number of genes enriched in each GO term. The rich factor is the ratio of the number of enriched DEGs to the total number of annotated genes in the GO term and is directly proportional to the degree of enrichment. The FDR is the expected proportion of false positives among all the significant results; the closer the FDR value is to zero, the more likely the significant results are likely to be true positives. PPI network functional enrichment analysis was performed using STRING 11.0

(https://string-db.org/). The STRING results were saved in tab-separated values (TSV) format, and the TSV file was retained and imported into Cytoscape software (version 3.9.1; bytesin.com/software/Cytoscape/) to visualize the relevant PPI networks. Clusters of networks were detected using the MCODE Cytoscape plugin (version 1.5.1) (25). The hub or core genes among the DEGs in the PPI network were identified using the CytoNCA Cytoscape plugin (version 2.1) (26).

Antibodies and inhibitors. The antibodies used in this study are listed in Table SI, along with the concentrations at which they were used. The following inhibitors were used: Picropodophyllin (PPP; cat. no. HY-15494; MedChemExpress) as an inhibitor of IGF1 receptor (IGF1R) activity (27-29); and GSK650394 (cat. no. HY-15192; MedChemExpress), as an inhibitor of serum/glucocorticoid regulated kinase 1 (SGK1) activity (30,31).

Reverse transcription-quantitative PCR (RT-qPCR). Total RNA was extracted from cells using TRNzol Universal Reagent (cat. no. DP424; Tiangen Biotech Co., Ltd.). Complementary DNA was synthesized from the RNA using the HiFiScript cDNA Synthesis Kit (cat. no. CW2569; CoWin Biosciences) under the following conditions: 42°C for 15 min and 85°C for 5 min. qPCR analysis was then performed using 2X UltraSYBR Mixture (cat. no. CW0957; CoWin Biosciences) on a CFX96 system (Bio-Rad Laboratories, Inc.) with the appropriate primers (Table SII). The qPCR conditions were as follows: 95°C for 10 min as the initial activation step, followed by 40 cycles of 95°C for 15 sec for denaturation and 60°C for 60 sec for annealing. The mRNA expression levels were calculated using the $2^{-\Delta\Delta Cq}$ relative quantification method (32). The expression level of each target gene was normalized to that of b-actin mRNA in the same sample.

Enzyme-linked immunosorbent assay (ELISA). Cells were plated in a 24-well plate at a density of 1×10^6 cells/well and incubated overnight to achieve 100% confluency. After discarding the culture supernatant, the cells were washed with phosphate-buffered saline (PBS) and cultured overnight in serum-free medium. The culture supernatant was then collected to measure the IGF1 levels using a mouse IGF1 (mIGF1) ELISA kit (cat. no. EK0378; Boster Biological Technology), following the manufacturer's instructions. The absorbance of the samples was measured at 450 nm using an Infinite M200 microplate reader (Tecan Group, Ltd.).

Cell counting assay. Cell proliferation was measured using a Cell Counting Kit-8 (CCK-8; cat. no. HY-K030; MedChemExpress), following the manufacturer's instructions. The absorbance of the samples at 450 nm was measured using an Infinite M200 microplate reader (Tecan Group, Ltd.).

Protein extraction and western blotting (WB). Control-L929 and MCT4-L929 cells were seeded into 6-cm dishes and incubated in the presence or absence of recombinant mIGF1 (cat. no. 50437-MNAY; Sino Biological, Inc.) at a concentration of 500 pg/ml for 1 h or inhibitors (300 nM PPP/5 μM GSK650394) for 2 h in serum-free medium at 37°C. The cells were serum-free starved overnight prior to treatment with mIGF1 or inhibitor. After incubation, cells were collected using a scraper, incubated on ice for 15 min, and lysed using radioimmunoprecipitation assay lysis buffer (cat. no. P0013C; Beyotime Institute of Biotechnology) with 1 mM protease inhibitor cocktail (cat. no. 05892970001; Roche Diagnostics, GmbH) and 1 mM phosphatase inhibitors (cat. no. 4906845001; Roche Diagnostics, GmbH). The lysate was centrifuged at 10,000 x g for 10 min. The protein concentration in the supernatant was quantified using a bicinchoninic acid assay kit (cat. no. AR0197A; Wuhan Boster Biological Technology, Ltd.).

To perform WB, lysates (15-50 μg/lane) were resolved using sodium dodecyl sulfate-polyacrylamide gel electrophoresis with a 12 (all proteins except IGF1) or 15% (for IGF1) gel. The resolved proteins were transferred to a 0.45-μm polyvinylidene difluoride membrane (cat. no. IPFL00010; Merck KGaA). To reduce background staining, the membrane was blocked with 5% bovine serum albumin in Tris-buffered saline containing 0.1% Tween 20 (TBST) for 1 h at room temperature. Next, the membrane was incubated with primary antibodies overnight at 4°C. After washing with TBST buffer, the membrane was incubated with horseradish peroxidase-conjugated anti-mouse (cat. no. 31430; Invitrogen; Thermo Fisher Scientific, Inc.; 1:5,000) or anti-rabbit (cat. no. 31460; Invitrogen; 1:5,000) secondary antibodies for 1 h at room temperature. Protein bands were visualized using enhanced chemiluminescence (cat. no. KGP1127; Nanjing KeyGen Biotech Co., Ltd.) with 5200 Multi Automatic Chemiluminescence (Tanon Science and Technology Co., Ltd.) and quantified using ImageJ v1.5.1 software (National Institutes of Health).

Cell migration assay. The wound healing assay, which mimics *in vivo* cell migration, is based on the observation of cell migration into a 'wound' that is generated in a cell monolayer (33). To form a confluent monolayer, 1×10^6 cells/well were seeded in a 24-well plate and incubated overnight to achieve 100% confluency. A wound was generated at the midline of each culture by scraping the confluent cells with a 200-μl pipette tip. Next, the cell monolayer was gently washed with PBS to remove the detached cells and incubated with fresh serum-free medium. In each experiment, a first image (0 h) was immediately captured under a light microscope (Leica Microsystems GmbH), and a second image was captured in the same manner after 48 h. The closure of the wound was measured using Image-Pro Plus analysis software (Media Cybernetics, Inc.). The migration rate was calculated using the following formula: Migration rate (%)=[(average wound width at 0 h-average wound width at 48 h)/average wound width at 0 h] x100.

For migration promotion or inhibition studies, the same protocol was used, with the exception that before wounds were generated, the cells were treated with serum-free medium overnight, and after the wounds were generated, mIGF1 (500 pg/ml for 1 h at 37°C), PPP (300 nM for 2 h at 37°C) or GSK650394 (5 μM for 2 h at 37°C) was added to the serum-free medium. Cell proliferation was measured using the aforementioned CCK-8 kit.

Lentivirus system-mediated knockdown of IGF1. BLOCK-iT™ RNAi Designer (https://rnaidesigner.thermofisher.com/rnaiexpress/) was used to design IGF1 short hairpin (sh) sequences. Three gene sequences were synthesized (Genewiz, Inc.): IGF1

sh1: 5'-GCCTCTGTGACTTCTTGAAGACGAATCTTC
AAGAAGTCACAGAGGC-3'; IGF1 sh2: 5'-GCTCTTCAG
TTCGTGTGTGGACGAATCCACACACGAACTGAAGAG
C-3'; and IGF1 sh3: 5'-CAGGCATTGTGGATGAGTGTTCGA
AAACACTCATCCACAATGCCTG-3'. These sequences
were cloned into an LV-U6-MSC-CMV-ZsGreen-PGK-PURO
vector (Hanheng Biotechnology Co., Ltd.) for lentiviral
packaging. The vector was also used for lentiviral pack-
aging as a knockdown control (shControl). The lentiviral
plasmids shControl and IGF1 sh1-3 were transfected into
293T cells (ATCC) using a LipoFiter™ transfection reagent
(cat. no. HB-TRIF-1000; Hanheng Biotechnology Co., Ltd.).

A total of 25 μg lentiviral plasmid was used for transfec-
tion. The lentivirus, packaging plasmid, and envelope plasmid
were used in a ratio of 2:2:1. After 6 h of transfection at 37°C,
the medium was replaced with complete medium (CSC03-CL
medium containing 10% FBS), and ZsGreen protein expres-
sion was observed 48 and 72 h after transfection. The viral
supernatant was removed after 72 h and the viral stock was
obtained by ultracentrifugation at 100,000 x g for 2 h at 4°C.

MCT4-L929 (4D11) cells were seeded at a density of
$1x10^4$ cells/well in a 96-well plate and incubated overnight.
Then, the culture supernatant was removed, 50 μl/well
lentivirus stock solution was added, and 50 μl complete
medium (CSC03-CL medium with 10% FBS) was added
after 4 h. Lentiviral transfection was performed using
a multiplicity of infection of 50. The virus-containing medium
was replaced with 100 μl/well complete medium after 24 h.
ZsGreen expression was observed 48 h after lentiviral
infection, and puromycin (10 μg/ml) was added to the cell
supernatant. Plates were then returned to the incubator for
2 weeks. Clones were sub-cultured in 24- or 6-well plates and
used for subsequent experiments.

Statistical analysis. Origin (Electronic Arts Inc.) was used
to generate volcano plots and GO/KEGG bubble diagrams.
Statistical analyses were performed using GraphPad Prism
software version 8.0.1 (GraphPad Software; Dotmatics).
Two-tailed unpaired t-tests were used to compare results
between two groups. One-way ANOVA or two-way ANOVA
with Tukey's post hoc test was used to compare results among
more than two groups. Correlation was assessed by Pearson's
coefficient. P<0.05 was considered to indicate a statistically
significant difference.

Results

Overview of RNA-Seq. Sequencing the three MCT4-L929 cell
lines (3E10, 4D11 and 8E4) and three control-L929 cell lines
(C5, H9 and 2H6) on an Illumina platform yielded an average
of 45,975,435 clean reads per library. The data quality analysis
revealed that the Q20 and Q30 ratios were >95 and >90%,
respectively. The total_mapped and uniquely_mapped ratios
were both >95%, indicating good data quality (Table SIII).

Transcriptome de novo assembly. Two groups of cells from
each cell line were subjected to correlation analysis to ensure
biological reproducibility within each group. Pearson's
correlation test was used to measure the correlation of gene
expression levels [fragments per kilobase of exon per million
mapped fragments (FPKM)] among the six cell lines (Fig. 1A).
A strong correlation coefficient (0.8-1.0) indicates high
reproducibility among samples within biological replicates.
Conversely, a correlation coefficient lower than 0.8 indicates
low reproducibility among samples in the same cohort.

The RNA-seq data of MCT4-L929 (3E10, 4D11 and 8E4)
and control-L929 (C5, H9 and 2H6) cells were normalized
using FPKM values. In total, 872 DEGs were identified with
|log$_2$FC|>1 and P<0.05; these comprised 337 upregulated
and 535 downregulated genes. The results are displayed in a
bar graph (Fig. 1B) and volcano plot (Fig. 1C). A clustering
heatmap was prepared to present a visual comparison of DEGs
between the MCT4-L929 and control-L929 cells (Fig. 1D).
In the GO and KEGG analyses, the top 15 GO terms with
the smallest FDR values are shown in Fig. 1E and the top 15
KEGG pathways with the smallest FDR values are shown in
Fig. 1F. The most enriched KEGG pathway is 'pathways in
cancer', suggesting that the upregulated expression of MCT4
may promote the carcinogenesis of L929 cells.

Analysis and identification of DEGs. The top three scoring
clusters in the PPI network according to the MCODE analysis
are listed in Table SIV. These clusters are shown in Fig. 2A-C,
where the nodes represent proteins and the edges represent
the association between proteins. The first-ranked network,
cluster 1, consists of 32 nodes and 155 edges, making it the
largest and potentially most impactful network. As a result,
this network was chosen for further examination. Table SV
lists the 32 genes of cluster 1 ranked by their betweenness
value obtained using CytoNCA. A higher betweenness value
indicates a higher likelihood of a gene being the core gene
in the PPI network. The size of each gene cluster was sorted
based on the betweenness value.

The mRNA levels of all genes in cluster 1 were subjected to
pairwise comparison. The fold change was determined as the
ratio of expression in the MCT4-L929 and control-L929 groups
according to the RNA-seq data (Fig. 2D). The transcription of
Serpina3f and *Serpina3i* in MCT4-L929 cells and that of puri-
nergic receptor P2Y14 (*P2ry14*) in control-L929 cells was low
(close to zero). Therefore, the fold change values of these three
genes were not calculated. The expression levels of all genes
in cluster 1 were verified using RT-qPCR (Fig. 2E). *P2ry14*
and *Igf1* exhibited large differences in expression between the
MCT4-L929 and control-L929 cells, which is consistent with
the RNA-seq results. Therefore, *P2ry14* and *Igf*1 were selected
as the two candidate target genes for further investigation.

P2RY14 is a UDP-glucose P2Y purinergic receptor that
plays a crucial role in signaling through G-protein-coupled
receptors and peptide ligand-binding receptors (34). It is asso-
ciated with various biological processes, including immune
responses, tumorigenesis and cell senescence (35,36). Studies
have shown that P2RY14 expression is significantly down-
regulated in head and neck squamous cell carcinoma and lung
cancer, and the higher expression of P2RY14 is associated with
an improved prognosis in patients with these cancers (37,38).
Acute leukemia cells that are resistant to PI3K/mTOR inhibi-
tion have been found to exhibit an upregulation of P2RY14,
which plays a role in patient survival and is associated with
activation of ERK signaling; however, PI3K/mTOR signaling
is not downstream of P2RY14 (39). In the formation and
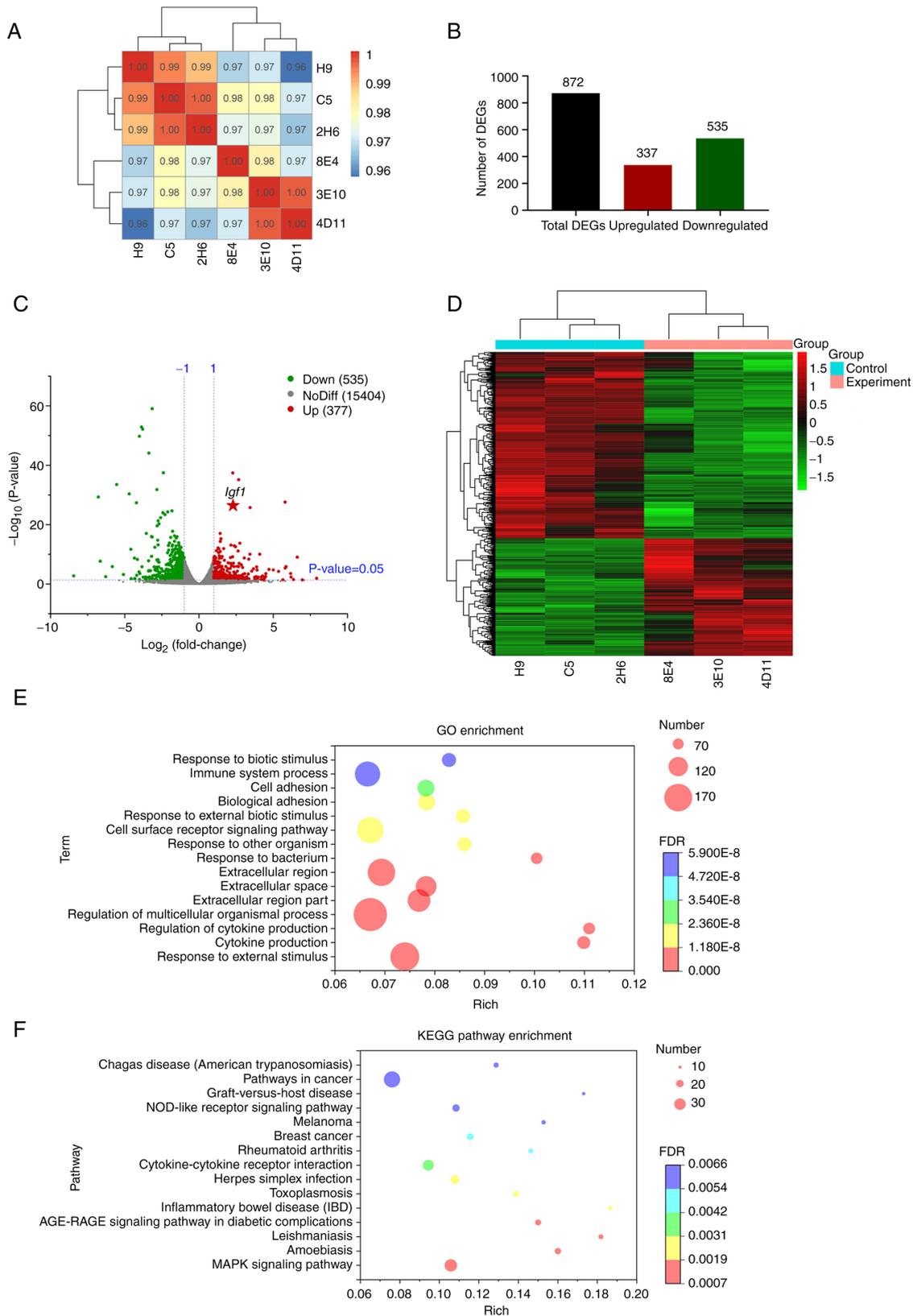
Figure 1. Transcriptome data analysis. (A) Sample correlation analysis. The left and upper sides indicate sample clustering, while the right and lower sides of the figure are cell line names. Different colors of the squares represent the strength of the correlation between the two corresponding samples. (B) Bar chart showing the number of upregulated and downregulated DEGs. (C) Volcano plot of DEGs in which the x-axis represents $\log_2$ |fold change| for MCT4-L929/control-L929 and the y-axis shows the $\log_{10}$ (P-value). The two vertical dashed lines in the figure indicate the two-fold expression difference threshold, while the horizontal dashed line indicates the P=0.05 threshold. The red and green dots represent upregulated and downregulated genes, respectively. The gray dots represent genes that are not significantly and differentially expressed. (D) Heatmap of DEGs in which each column is a cell line and the y-axis represents DEGs. The colors indicate the expression levels of the DEGs; red and green represent upregulated and downregulated genes, respectively. (E) GO enrichment and (F) KEGG enrichment. The color of each bubble represents the P-value, while the size represents the number of DEGs in the GO or KEGG term. The x-axis shows the rich factor, which represents the ratio of DEGs vs. total genes in the pathway that is measured. DEGs, differentially expressed genes; GO, Gene Ontology; KEGG, Kyoto Encyclopedia of Genes and Genomes; Igf1, insulin-like growth factor 1; NoDiff, no difference.
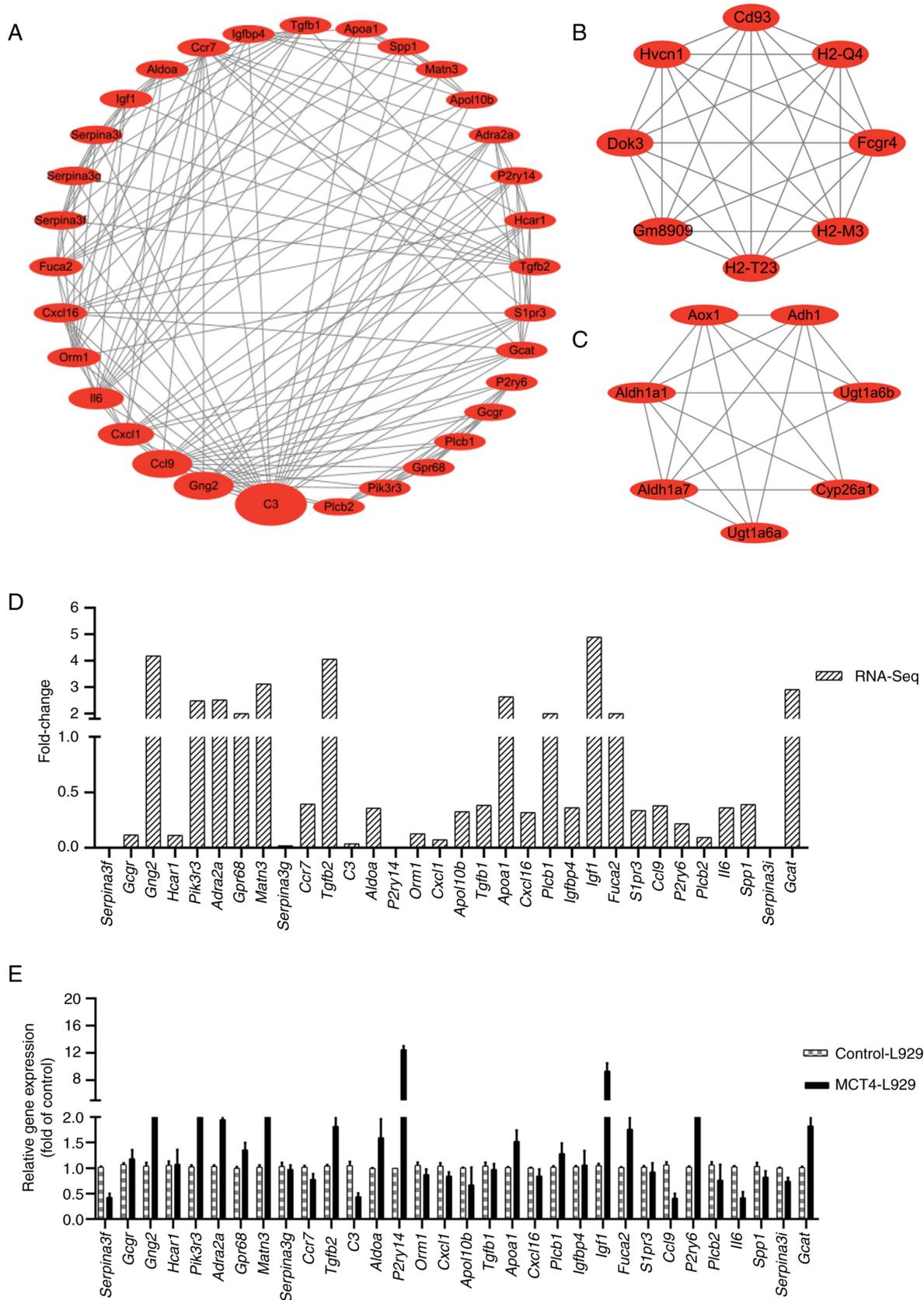
Figure 2. PPI networks of DEGs and RNA-Seq analysis of selected cluster genes. (A-C) PPI clusters of the top 3 DEGs. (A) Cluster 1, (B) cluster 2 and (C) cluster 3. Each node represents a protein, and the lines between proteins indicate predicted interactions or associations. The size of each gene node is sorted according to the betweenness value. (D) RNA-seq analysis of the expression ratio of cluster 1 genes in MCT4-L929 cells over control-L929 cells. Fold change >1 indicates that the transcription level in CT4-L929 cells was higher than that in control-L929 cells. (E) Reverse transcription-quantitative PCR analysis of the expression of cluster 1 genes. Fold of control >1 indicates that the expression of the gene in MCT4-L929 cells was higher than that in control-L929 cells. The transcription level of target genes in MCT4-L929 cells was normalized to that in control-L929 cells. The means of the data from three cell lines in each group are shown, and each error bar represents one standard deviation. PPI, protein-protein interaction; DEGs, differentially expressed genes; RNA-seq, RNA sequencing; MCT4, monocarboxylate transporter 4.

development of gastrointestinal cancers, P2Y14 triggers numerous mitogen-activated protein kinases (MAPKs), Src family kinases and downstream protein kinases (40). Furthermore, in stem/progenitor cells, P2RY14 inhibits cell senescence through a mechanism involving reactive oxygen species, p38 MAPK/JNK and p16/Rb (35).

IGFs family members and their receptors constitute an important growth regulatory system under physiological conditions. However, under pathological conditions, IGFs contribute to tumorigenesis owing to their powerful pro-growth and anti-apoptotic effects (41,42). IGF1 expression is upregulated in tumors (43), and promotes the growth and metastasis of various tumors, including Wilms tumor (44), papillary thyroid cancer (45), colorectal cancer (46), glioma (47) and cervical cancer (48).

Cytoscape analysis indicates that *Igf1* has a higher betweenness value than *P2ry14* (Table SV). Additionally, the aforementioned studies have shown that P2RY14 is downregulated in several types of tumors and that higher expression levels are associated with better patient prognosis while, by contrast, IGF1 and MCT4 are upregulated in tumors and promote tumor growth and metastasis. On the basis on these findings, it was decided to focus the present investigation on *Igf1*.

MCT4 activates the IGF1/IGF1R/PIK3R3/SGK1 axis. WB analysis indicated that MCT4 upregulated the expression level of IGF1 (Fig. 3A and B). The upregulation of IGF1 levels in the MCT4-L929 culture supernatant was demonstrated using mIGF1 ELISA test. As the cells were cultured in serum-free medium, no exogenous IGF1 was present. The difference in the IGF1 concentration between the MCT4-L929 and control-L929 cells was 150-250 pg/ml (Fig. 3C). Analysis using the CCK-8 assay revealed that the number of MCT4-L929 and control-L929 cells was not significantly different (Fig. S1A).

The function of IGF1 is primarily mediated through the IGF1R (49,50). The IGF1R has been reported to be involved in aberrant tumor growth and malignancy *in vitro* (51). Therefore, the mRNA levels of *Igf1r* and key genes downstream of activated IGF1R were evaluated. The *Igf1r* mRNA levels in MCT4-L929 cell lines were found to be higher than those in control-L929 cell lines (Fig. 3D), which we hypothesize may be attributed to upregulated IGF1 expression.

Two major downstream pathways of IGF1/IGF1R are the Ras/Raf and phosphoinositide 3-kinase (PI3K) pathways (52). PI3K regulatory subunit 3 (*Pik3r3*), which encodes the PI3K regulatory subunit p55γ (53), is a key gene in cluster 1 (Fig. 2A) and its mRNA level is upregulated in MCT4-L929 cell lines (Fig. 3D). Therefore, it was speculated that the PI3K pathway may be the key pathway downstream of IGF1/IGF1R. PIK3R3 is reported to be involved in the migration and invasion of various cancers, including glioma (54), oral carcinoma (55) and melanoma (56). AKT is commonly reported as a downstream mediator of PI3K (57). However, the RNA-seq analysis revealed that *Akt* was not a DEG while *Sgk1* was differentially expressed between the MCT4-L929 and control-L929 cell lines. SGK1 is a member of the cAMP-dependent, cGMP-dependent and protein kinase C family of serine/threonine kinases, which shares a large homologous sequence and kinase function with the AKT family. Additionally, SGK1 is a downstream effector

of PI3K that acts in parallel to AKT (57) and is upregulated in most cancers (58). SGK1 overexpression has been reported to promote cell migration and invasion in various cancers, including colorectal cancer (59), lung adenocarcinoma (60) and prostate cancer (61).

The transcription of several effector genes downstream of IGF1/IGF1R signaling was quantified using RT-qPCR (Fig. 3D). The *Pik3r3* and *Sgk1* mRNA levels in MCT4-L929 cells were higher than those in control-L929 cells. However, the mRNA levels of *Akt1*, *Akt2* and *Akt3* were not significantly different between the MCT4-L929 and control-L929 cells. These findings are consistent with the RNA-seq data. The protein levels of IGF1, IGF1R, PIK3R3, SGK1, AKT1/2/3 and their phosphorylation levels, with the exception of IGF1 phosphorylation, were analyzed using WB. The protein levels of IGF1, IGF1R, p-IGF1R, PIK3R3, p-PIK3R3, SGK1 and p-SGK1 in the MCT4-L929 cells were higher than those in the control-L929 cell lines (Fig. 3E and F). As the expression levels of both total and phosphorylated levels of IGF1R, PIK3R3, and SGK1 were increased in MCT4-L929 cells compared with control-L929 cells, the ratios of phosphorylated to total proteins did not show a significant difference between MCT4-L929 and Control-L929 cells (Fig. 3G). Therefore, it was speculated that the overexpression of MCT4 may promote the migration of L929 cells via activation of the IGF1/IGF1R/PIK3R3/SGK1 pathway.

IGF1 promotes the migration of control-L929 cells. Control-L929 cell lines (C5, H9, and 2H6) were treated with mIGF1 to simulate the effect of MCT4 overexpression. The migration rate of the control-L929 cells treated with 500 pg/ml mIGF1 was significantly upregulated and similar to that of MCT4-L929 cells (Fig. 4A and B). Analysis using the CCK-8 kit revealed that the number of MCT4-L929 and control-L929 cells was not significantly different (Fig. S1A). The expression and phosphorylation of proteins in the IGF1R/PIK3R3/SGK1 axis were examined in control-L929 cells treated with 500 pg/ml mIGF1 for 1 h. As in Fig. 4C and D, the levels of IGF1R, p-IGF1R, p-PIK3R3 and p-SGK1 in IGF1-stimulated cells were comparable to those in MCT4-L929 cells. Phosphorylated/total protein ratios were shown in Fig. 4E. In the blank group, the ratio of phosphorylated protein to total protein showed no significant difference between MCT4-L929 and control-L929 cells as the expressions of both total and phosphorylated proteins of IGF1R, PIK3R3, and SGK1 were increased in MCT4-L929 cells compared with control-L929 cells (Fig. 4E). In the mIGF1 group, the ratio of phosphorylated IGF1R and PIK3R3 to their corresponding total proteins showed no significant difference between MCT4-L929 and control-L929 cells, but the ratio of phosphorylated SGK1 to total protein in MCT4-L929 cells was significantly lower than that in control-L929 cells, which could be attributed to the notable changes in SGK1 and p-SGK1.

Conversely, the expression of IGF1 was knocked down in the MCT4-L929 cell line 4D11 using a lentivirus system. The migration-promoting effect of MCT4 in the L929 cells was mitigated to varying degrees according to the degree of IGF1 knockdown (Fig. S2). The knockdown of IGF1 expression in the MCT4-L929 (4D11) cells by IGF1 sh1-3 was evaluated. The results indicated that IGF1 sh-2 and particularly IGF1 sh-3 decreased the expression level of IGF1. The migration rate of the MCT4-L929 cells (4D11) treated with IGF1 sh-2 was
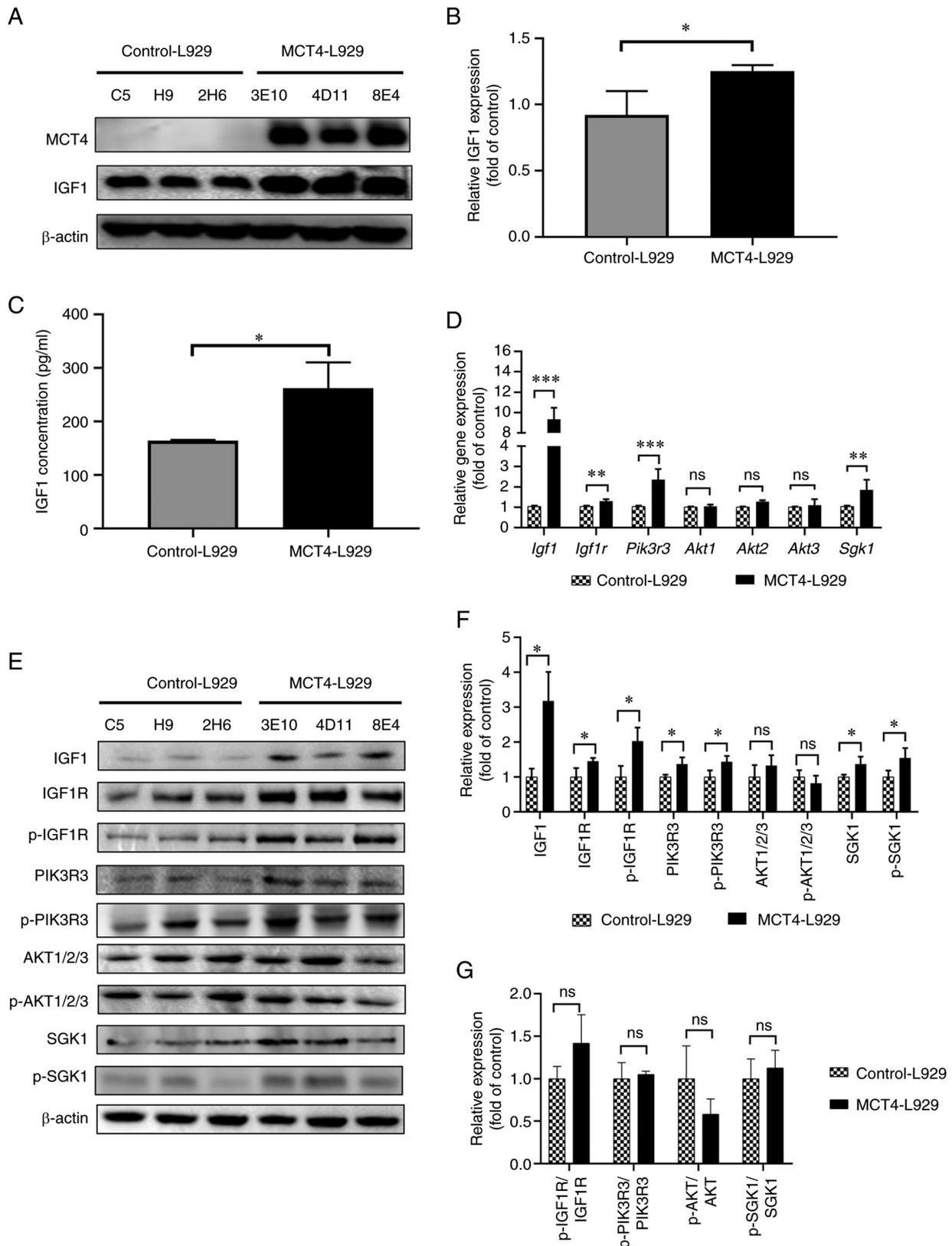
Figure 3. MCT4 activates the IGF1/IGF1R/PIK3R3/SGK1 axis. (A) WB analysis of MCT4 and IGF1 levels in control-L929 and MCT4-L929 cell lines using β-actin as a loading control and (B) semi-quantification of the WB results. The expression of IGF1 was normalized to that of β-actin. (C) IGF1 concentration in the supernatant of MCT4-L929 and control-L929 cell lines as quantified using an enzyme-linked immunosorbent assay. (D) The mRNA levels of selected genes in the IGF1/IGF1R pathway in MCT4-L929 and control-L929 cells as quantified using reverse transcription-quantitative PCR. Transcription levels in MCT4-L929 cells were normalized to those in control-L929 cells. (E) WB analysis of IGF1, IGF1R, PIK3R3, AKT1/2/3 and SGK1 expression levels and the phosphorylation of IGF1R, PIK3R3, AKT1/2/3 and SGK1 and (F) semi-quantification of the WB results. (G) Phosphorylated/total protein ratio. The expression levels in MCT4-L929 cells were normalized to those in control-L929 cells. The means of the data from three cell lines in each group are shown, and each error bar represents one standard deviation. Differences between groups were analyzed using two-tailed unpaired t-tests. $^*P<0.05$, $^{**}P<0.01$ and $^{***}P<0.001$. ns, not significant; MCT4, monocarboxylate transporter 4; IGF1, insulin-like growth factor 1; IGF1R, IGF1 receptor; PIK3R3, phosphoinositide 3-kinase regulatory subunit 3; SGK1, serum/glucocorticoid regulated kinase 1; WB, western blotting; p-, phosphorylated.
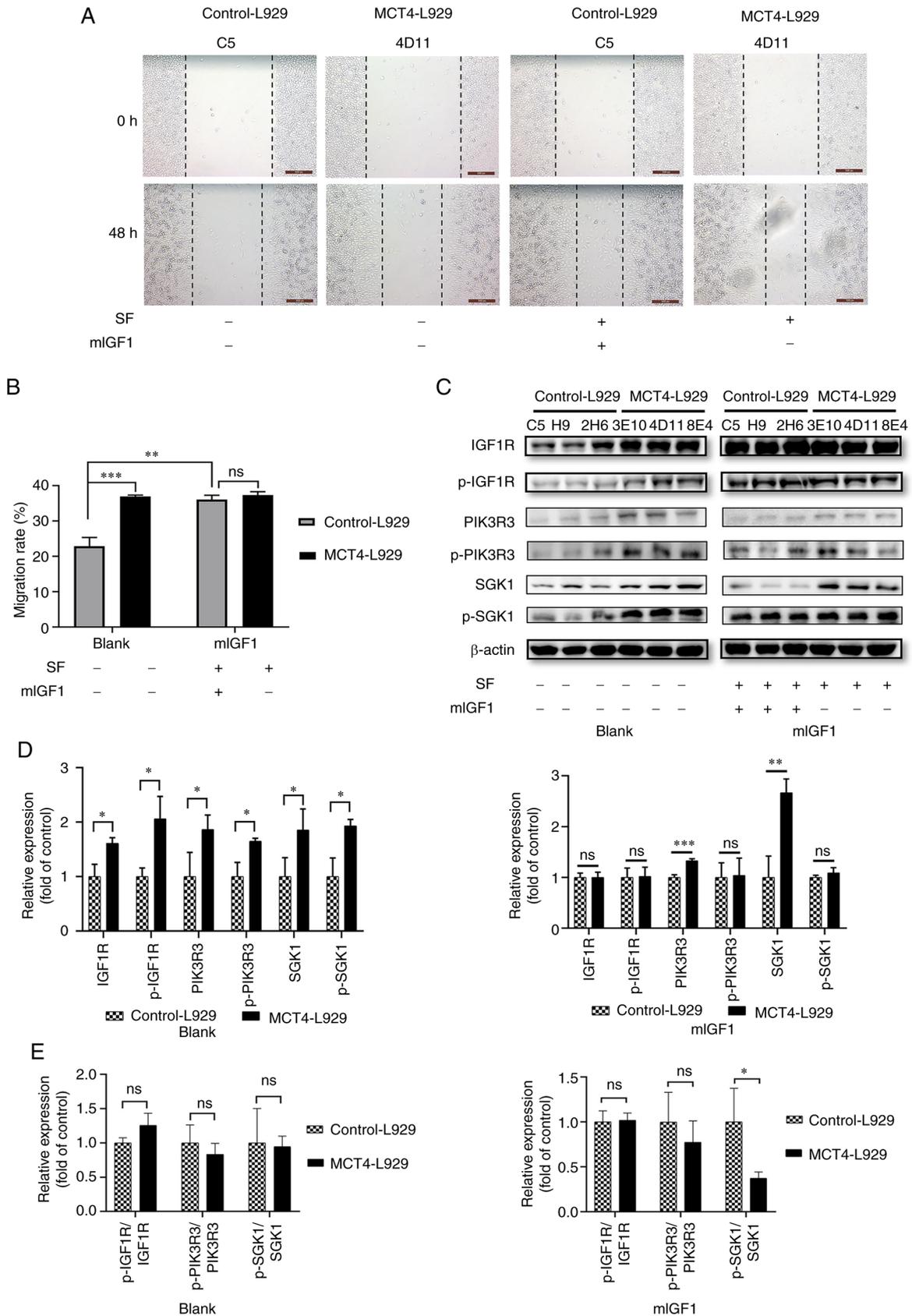
Figure 4. IGF1 promotes the migration of control-L929 cells. (A) Representative wound healing images of the control-L929 and MCT4-L929 cells treated with or without SF and mIGF1 and (B) quantified wound healing results. (C) Western blot analysis of the expression levels of IGF1, IGF1R, PIK3R3 and SGK1 and the phosphorylated forms of IGF1R, PIK3R3 and SGK1 in control-L929 and MCT4-L929 cells supplemented with or without SF and mIGF1 using β-actin as a loading control and (D) semi-quantification of the results. The expression level of target genes in MCT4-L929 cells was normalized to that in control-L929 cells. (E) Phosphorylated/total protein ratio. The means of the data from three cell lines in each group are shown, and each error bar represents one standard deviation. Differences between groups were analyzed using two-tailed unpaired t-tests. $^{*}P<0.05$, $^{**}P<0.01$ and $^{***}P<0.001$. ns, not significant; IGF1, insulin-like growth factor 1; MCT4, monocarboxylate transporter 4; SF, serum-free starvation overnight before mIGF1 treatment; mIGF1, mouse IGF1; IGF1R, IGF1 receptor; PIK3R3, phosphoinositide 3-kinase regulatory subunit 3; SGK1, serum/glucocorticoid regulated kinase 1; p-, phosphorylated.

downregulated and was significantly downregulated by IGF1 sh-3 to a level similar to that of control-L929 cells (2H6). CCK-8 assay indicated that viability of L929 cells was not significantly affected by the knockdown of IGF1 (Fig. S2B). The phenotypes of the IGF1-supplemented control-L929 cells and IGF1 knock-down MCT4-L929 cells indicate the critical role of IGF1 in the regulation of L929 cell migration, suggesting that MCT4 may exert its cell migration-promoting function via IGF1.

Inhibition of IGF1R or SGK1 mitigates the migration-promoting effect of MCT4. To further examine whether MCT4 exerts its function through the IGF1/IGF1R pathway, the IGF1R inhibitor PPP and SGK1 inhibitor GSK650394 were used to block the functions of MCT4. The migration rate of MCT4-L929 cells treated with 300 nM PPP was significantly downregulated to a level similar to that of control-L929 cells (Fig. 5A and B). CCK-8 analysis revealed that the number of MCT4-L929 and control-L929 cells was not significantly different (Fig. S1B). WB analysis revealed that the phosphory-lation of IGF1R was significantly inhibited in the MCT4-L929 cells upon PPP treatment (Fig. 5C and D). In the blank group, the ratio of phosphorylated protein to total protein showed no significant difference between MCT4-L929 and control-L929 cells as the expressions of both total and phosphorylated proteins of IGF1R were increased in MCT4-L929 cells compared with control-L929 cells. In the PPP group, the ratio of phosphorylated IGF1R protein to total protein in MCT4-L929 cells was significantly lower than that in control-L929 cells, which could be attributed to the notable changes in IGF1R and p-IGF1R.SGK1 functions as an essential AKT-independent mediator of the PI3K/mTOR signaling pathway in cancer (62). The investigation of SGK1 in the present study is particularly important as the relationship between the PI3K-SGK1 pathway and cancer metastasis has rarely been reported. To the best of our knowledge, the only previous study that has examined this correlation demonstrated that dexamethasone enhances breast cancer lung metastasis through the PI3K-SGK1-connective tissue growth factor pathway (63). The migration rate of MCT4-L929 cells treated with 5 μM GSK650394 was signifi-cantly reduced to a level similar to that of the control-L929 cells (Fig. 6A and B). CCK-8 analysis revealed that the number of MCT4-L929 and control-L929 cells was not significantly different (Fig. S1C). The phosphorylation of SGK1 in the MCT4-L929 cells was significantly downregulated after GSK650394 treatment, whereas the expression of SGK1 was unaffected (Fig. 6C and D). In the blank group, the ratio of phosphorylated protein to total protein showed no significant difference between MCT4-L929 and control-L929 cells as the expressions of both total and phosphorylated proteins of SGK1 were increased in MCT4-L929 cells compared with control-L929 cells. In the GSK650394 group, the ratio of phosphorylated SGK1 to their corresponding total proteins also showed no significant difference between MCT4-L929 and control-L929 cells.

Discussion

In the present study, MCT4-overexpressing L929 cells were used to investigate the potential pathways and mechanisms through which MCT4 promotes cell migration. The results

revealed that MCT4 overexpression increases the transcript and protein levels of IGF1, the mechanism of which is unknown. The expression of IGF1 activates PIK3R3 and SGK1, which promote the migration of L929 cells. Therefore, it is suggested that one possible pathway through which MCT4 exerts its function is the IGF1/IGF1R/PIK3R3/SGK1 axis (Fig. 7).

Previous studies have demonstrated that silencing MCT4 in certain tumor cells can reduce the migration and invasion of the cells, but the mechanism by which MCT4 promotes migration is inconsistent in different tumor cell models (16,21,64,65). For instance, MCT4 is reported to promote tumor cell invasion and migration through the integrin β4-SRC-FAK and MEK-ERK pathways in oral squamous cell carcinoma (16). By contrast, MCT4 has been suggested to facilitate the metastasis of renal cancer cells through integrin β1 (64), while MCT4 has been demonstrated to promote hepatocellular migration via upregu-lation of the trafficking protein particle complex subunit 5 (TRAPPC5) gene (65). Furthermore, MCT4 has been shown to promote the invasion of prostate cancer cells via the regula-tion of invasion-associated genes, including VEGF, CD147, MMP2 and MMP9 (21). These findings are from studies in which MCT4 was silenced in one type of tumor cell, and the mechanism by which MCT4 promotes migration varies among the different tumor cell models. Silencing may sometimes be transient or incomplete; however, in our previous study, MCT4-L929 cell lines were generated by stable transfection and it was demonstrated that MCT4 promotes the migration and invasion of non-cancerous L929 cells (24). Therefore, it is suggested that the upregulated expression of MCT4 may promote the carcinogenesis of L929 cells. In the present study, the possible mechanism by which MCT4 promotes the migra-tion of L929 cells was investigated. In contrast to previous studies, the possible mechanism was studied via the over-expression of MCT4 rather than by silencing MCT4, which provides some new information on the promotion of tumor cell the migration and carcinogenesis by MCT4.

The present study systematically analyzed the transcrip-tome of three MCT4-L929 cell lines and compared it with that of three control-L929 cell lines. Based on subsequent validation studies, it is proposed that MCT4 may promote migration by upregulating the expression of IGF1. Generally, IGF1 activates its downstream pathway via the phosphorylation of IGF1R. In the present study, the results indicated that an increase in the expression of IGF1 may activate the downstream pathway by increasing the expression and phosphorylation of IGF1R. It has previously been shown that under hypoxic conditions, the expression level of IGF1 is significantly upregulated in pancreatic fibroblast cells and that of IGF1R is upregulated in pancreatic cancer cells under the same cancer microen-vironment, indicating a possible association between IGF1 and IGF1R expression (50). Although previous studies have reported that IGF1 or MCT4 promote tumor cell migration, the role of IGF1 in MCT4-mediated cell migration has not been reported. It has been shown that IGF1 promotes cell inva-sion and proliferation via activation of the IGF1/PI3K/AKT1 pathway (66) and can activate the PI3K/SGK1 pathway in cells (67). The role of SGK1 in MCT4-mediated cell migra-tion has not been reported. To the best of our knowledge, the present study is the first to report that MCT4 overexpression promotes cell migration by upregulating the expression of
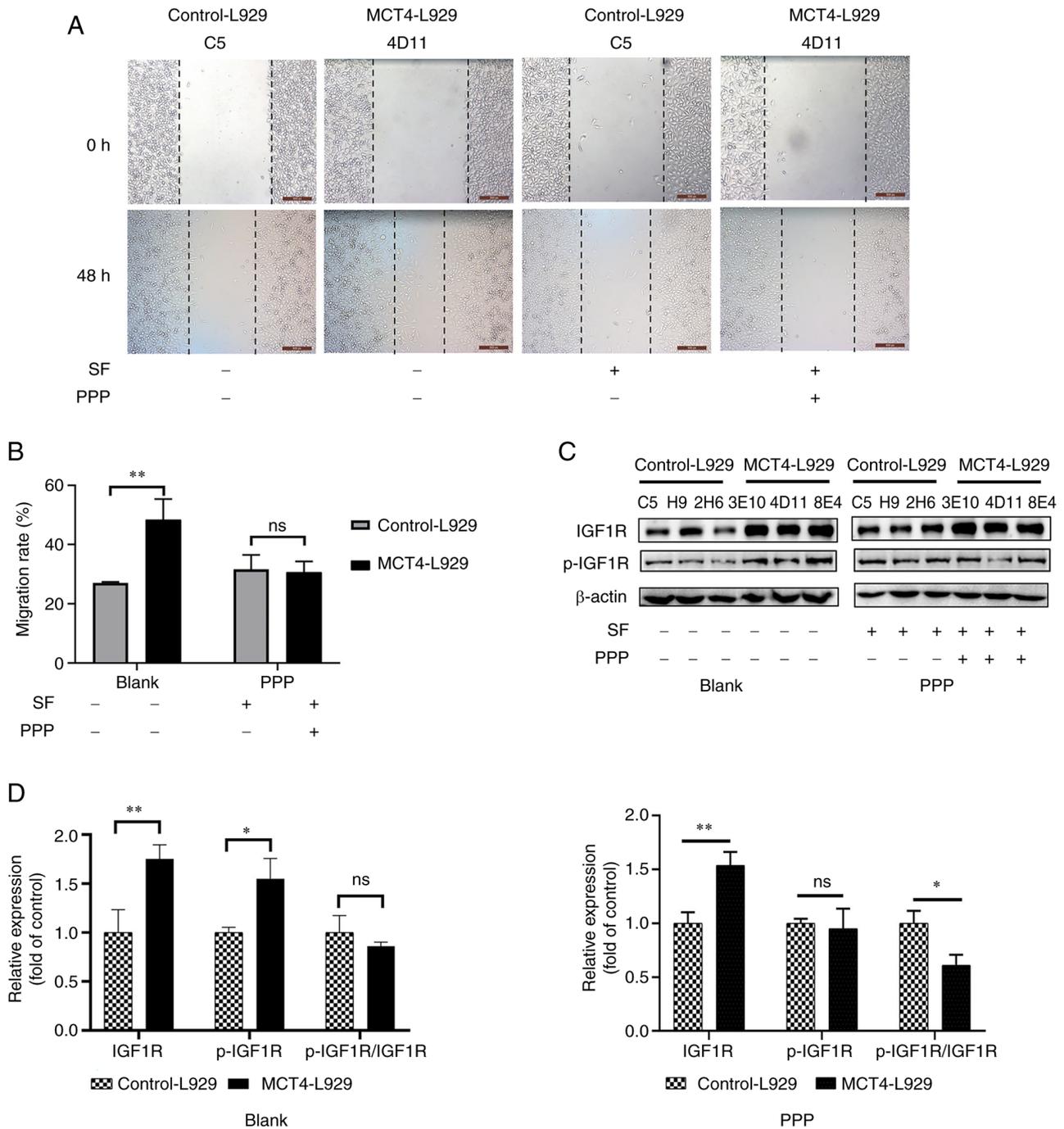
Figure 5. Inhibition of IGF1R mitigates the migration-promoting effect of MCT4. (A) Representative wound healing images of the control-L929 and MCT4-L929 cells treated with or without PPP and SF and (B) quantified wound healing results. (C) Western blotting analysis of IGF1R expression and phosphorylation in control-L929 and MCT4-L929 cells treated with or without SF and PPP using β-actin as a loading control and (D) semi-quantification and phosphorylated/total protein ratio. The protein levels in MCT4-L929 cells were normalized to those in control-L929 cells. The means of the data from three cell lines in each group are shown, and each error bar represents one standard deviation. Differences between groups were analyzed using two-tailed unpaired t-tests. $^*P<0.05$ and $^{**}P<0.01$. ns, not significant; IGF1R, insulin-like growth factor 1 receptor; MCT4, monocarboxylate transporter 4; PPP, picropodophyllin; SF, serum-free starvation overnight before PPP treatment; p-, phosphorylated.

IGF1 and activating the IGF1/IGF1R/PIK3R3/SGK1 axis. The findings of the present study may provide useful insights into the mechanism underlying MCT4-mediated cell migration and provide new ideas for the mechanistic investigation of MCT4-promoted tumor cell metastasis. The findings may also generate new perspectives on MCT4-mediated carcinogenesis, as promotion of the expression of IGF1 by MCT4 may mediate cell carcinogenesis. It is hypothesized that MCT4 may play

an important role in the early stages of cancer progression, in cells that are not already cancerous.

In the present study, the IGF1/IGF1R/PIK3R3/SGK1 axis was identified as a plausible pathway through which MCT4 promotes cell migration. This conclusion was achieved through the study of a panel of MCT4-overexpressing cell lines compared with control cell lines. Recently, a potent MCT4-specific inhibitor, MSC-4381, has been reported that
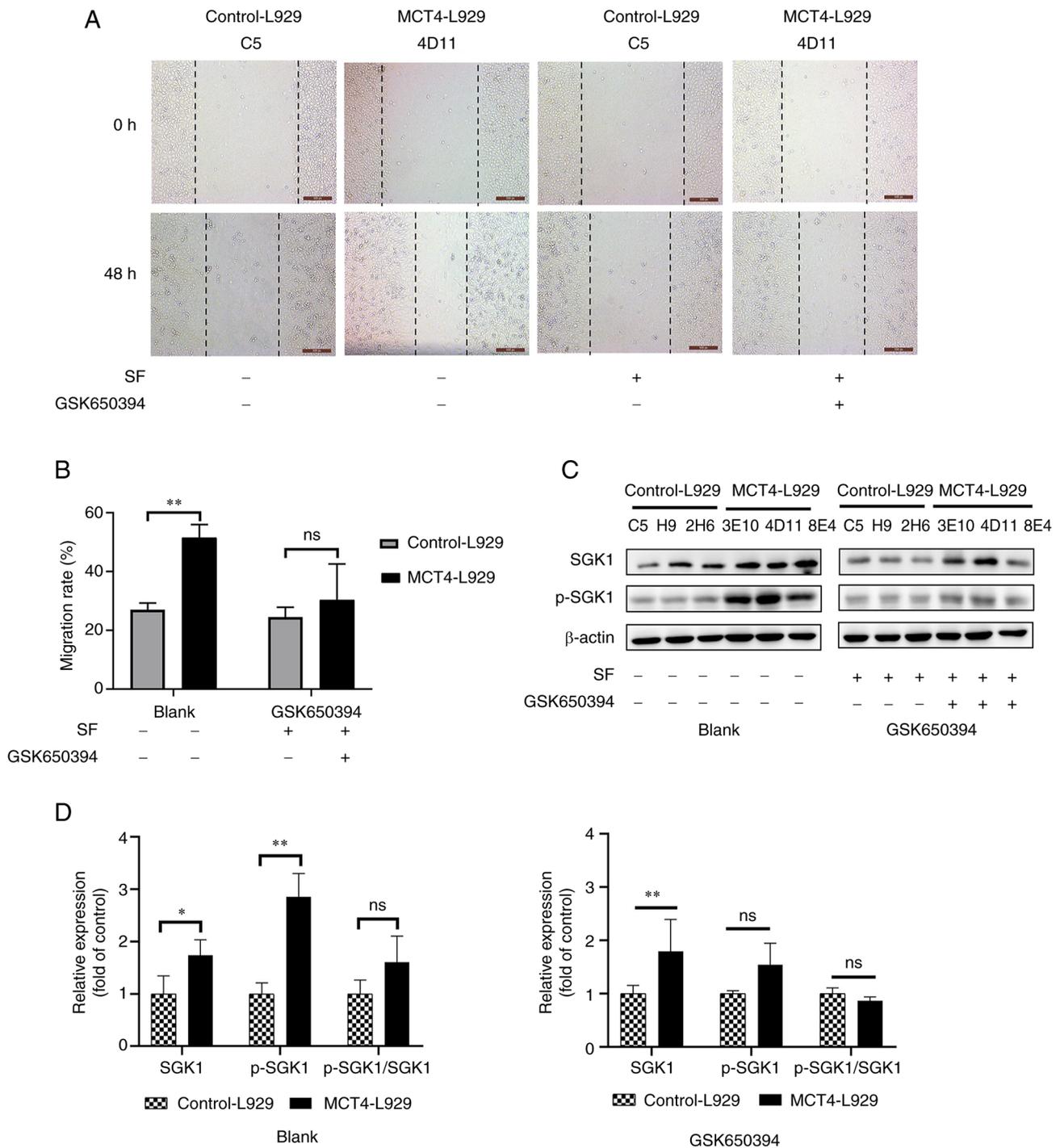
Figure 6. Inhibition of SGK1 mitigates the migration-promoting effect of MCT4. (A) Representative wound healing images of the control-L929 and MCT4-L929 cells treated with or without GSK650394 and (B) quantification of the wound healing results. (C) Western blotting analysis of SGK1 expression and phosphorylation in control-L929 and MCT4-L929 cells treated with or without SF and GSK650394 using β-actin was used as a loading control and (D) semi-quantification and phosphorylated/total protein ratio. The protein levels in MCT4-L929 cells were normalized to those in control-L929 cells. The means of the data from three cell lines in each group are shown, and each error bar represents one standard deviation. Differences between groups were analyzed using two-tailed unpaired t-tests. *P<0.05 and **P<0.01. ns, not significant; SGK1; serum/glucocorticoid regulated kinase 1; MCT4, monocarboxylate transporter 4; SF, serum-free starvation overnight before GSK650394 treatment; p-, phosphorylated.

effectively suppresses the efflux of lactate and decreases cell viability in cells with high MCT4 expression (68). It would be worthwhile to investigate if MSC-4381 is able to eradicate the function of MCT4 in activating the IGF1/IGF1R/PIK3R3/SGK1 axis. This investigation will be undertaken in future studies.

The lack of *in vivo* validation is one of the limitations of the present study. In previous studies, the knockdown of MCT4

expression has been shown to decrease the migration and invasion of lung cancer, oral squamous, hepatocellular carcinoma, pancreatic ductal adenocarcinoma, prostate cancer, glioma, bladder cancer and breast cancer cells (13,16-19,21-23). However, to date, there are only two relevant studies on the *in vivo* testing of MCT4 knockdown tumor cell lines. In one study, the knockout of MCT4 in the 5637 human bladder cancer cell line
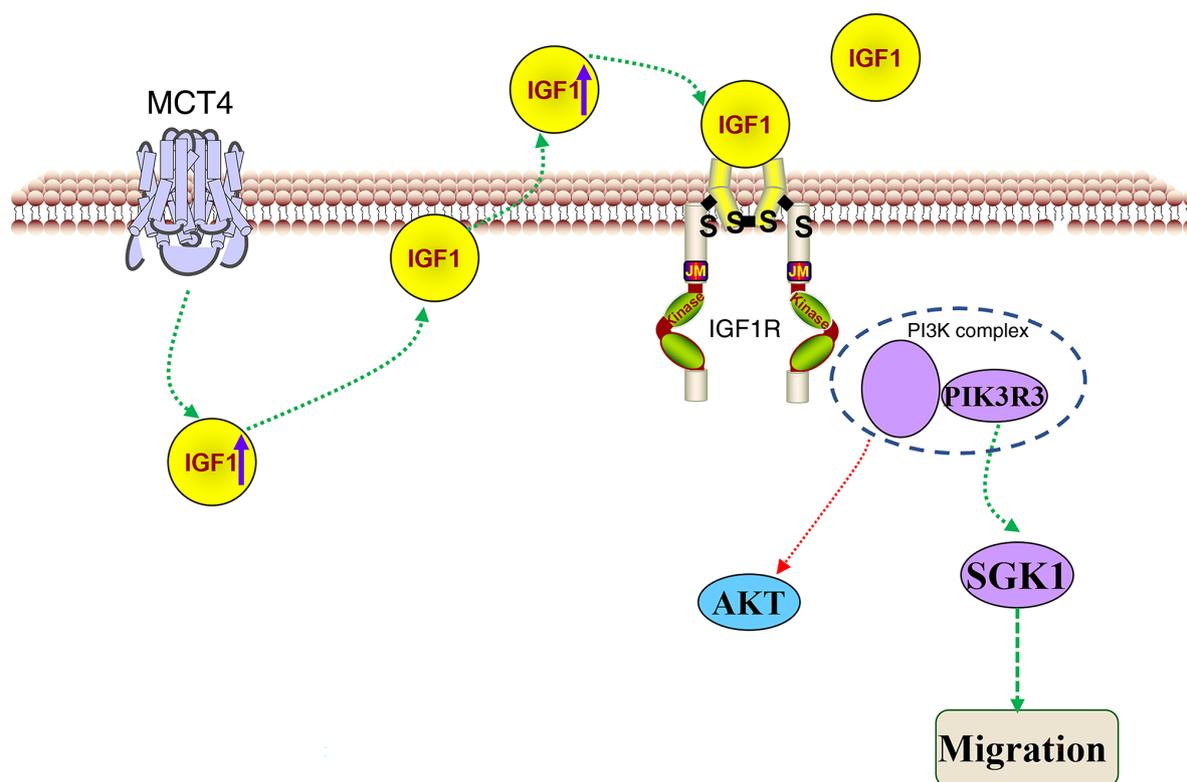
Figure 7. A schematic illustration showing the mechanism in which MCT4 drives the migration of non-cancerous L929 fibroblast cells via activation of the IGF1/IGF1R/PIK3R3/SGK1 axis. MCT4, monocarboxylate transporter 4; IGF1, insulin-like growth factor 1; IGF1R, IGF1 receptor; PIK3R3, phosphoinositide 3-kinase regulatory subunit 3; SGK1, serum/glucocorticoid regulated kinase 1.

resulted in a significant reduction in the tumorigenic ability of the cells in nude mice (17). In the other, TRAPPC5 expression was significantly downregulated following the knockdown of MCT4 in HCCLM3 highly metastatic liver cancer cells, and the knockdown of TRAPPC5 in HCCLM3 cells resulted in a significant reduction in the tumorigenicity of HCCLM3 cells in nude mice (65). Indeed, in a follow-up to the present study, it is planned to investigate the effect of IGF1 overexpression on the migration of MCT4-L929 cells *in vivo*. At present, a MCT4 knockout mouse model has been established which will be used to compare the migration capability of spontaneous tumors in knockout and wild-type mice. The *in vivo* results will be reported upon completion of the experiments.

IGF1 has been reported to promote cell proliferation and metastasis, and IGF1 exerts its function through activation of the PI3K/AKT or STAT3 pathways (44,45,66,69). However, in the present study, it was discovered that although MCT4 upregulates IGF1, the higher IGF1 expression did not increase the proliferation of the L929 cells. In addition, the mRNA levels of *Akt1*, *Akt2* and *Akt3* did not show any significant differences between the MCT4-L929 and control-L929 cells, which aligns with the results obtained from RNA-seq analysis. Furthermore, the protein levels of AKT1, AKT2 and AKT3, as well as their phosphorylation levels, exhibited no discernible variation between the cell lines. The discrepancy between the present observations and those of previous reports may originate from the difference in IGF1 concentration. The concentration of IGF1 reported to promote cell proliferation is generally in the range of 10-100 ng/ml (44,45,66,69). However, in the present study, the concentration of IGF1 in the

MCT4-L929 medium was only 150-250 pg/ml higher than that in the control-L929 medium, which is markedly lower than that required to accelerate proliferation.

The mechanism through which MCT4 increases the expression of IGF1 is unknown. However, there have been some interesting reports that may be relevant. It has been demonstrated that under hypoxic conditions, E74 like ETS transcription factor 3 (also known as epithelium-specific ETS transcription factor 1 and epithelial-restricted with serine box) promotes tumor angiogenesis via the upregulation of IGF1 expression and secretion and consequently improves endothelial cell proliferation and migration (70). In addition, it has been shown that IGF1 promotes the stability and expression of HIF1A (71), and TGF-β1 upregulates MCT4 expression via HIF1A under hypoxic conditions (72). Therefore, the mechanism by which MCT4 increases the expression of IGF1 is of academic interest and will be investigated in future studies.

Acknowledgements

Availability of data and materials

The RNA-seq raw datasets generated and analyzed during the current study are available in the National Center for

Biotechnology Information Sequence Read Archive (https://www.ncbi.nlm.nih.gov/bioproject/PRJNA859999). Other datasets generated and/or analyzed during the current study are available from the corresponding author on reasonable request.

Authors' contributions

NM and YZ conceived and designed the study. XZ, SW and YL performed the experiments and collected and analyzed the results. HZ, XH, YYu, YC, YYa, XM, HH, and MZ assisted with the experiments and data analysis. XZ and NM reviewed the literature and wrote the manuscript. XZ and NM confirm the authenticity of all the raw data. All authors read and approved the final version of the manuscript.

Ethics approval and consent to participate

Not applicable.

Patient consent for publication

Not applicable.

Competing interests

The authors declare that they have no competing interests.

References

1. Chaffer C and Weinberg R: A perspective on cancer cell metastasis. Science 331: 1559-1564, 2011.
2. Steeg PS: Tumor metastasis: Mechanistic insights and clinical challenges. Nat Med 12: 895-904, 2006.
3. Wu Y, Zhang T, Zhang X and Gao Q: Decoding the complexity of metastasis. Cancer Biol Med 19: 284-288, 2022.
4. Nakamura Y, Fujimoto M, Fukushima S, Nakamura A, Hayashida N, Takii R, Takaki E, Nakai A and Muto M: Heat shock factor 1 is required for migration and invasion of human melanoma in vitro and in vivo. Cancer Lett 354: 329-335, 2014.
5. Chiu WT, Shen SC, Chow JM, Lin CW, Shia LT and Chen YC: Contribution of reactive oxygen species to migration/invasion of human glioblastoma cells U87 via ERK-dependent COX-2/PGE(2) activation. Neurobiol Dis 37: 118-129, 2010.
6. Ishimura N, Isomoto H, Bronk SF and Gores GJ: Trail induces cell migration and invasion in apoptosis-resistant cholangio-carcinoma cells. Am J Physiol Gastrointest Liver Physiol 290: G129-G136, 2006.
7. Malla RR and Kiran P: Tumor microenvironment pathways: Cross regulation in breast cancer metastasis. Genes Dis 9: 310-324, 2022.
8. Mosier JA, Schwager SC, Boyajian DA and Reinhart-King CA: Cancer cell metabolic plasticity in migration and metastasis. Clin Exp Metastasis 38: 343-359, 2021.
9. Hipolito A, Martins F, Mendes C, Lopes-Coelho F and Serpa J: Molecular and metabolic reprogramming: Pulling the strings toward tumor metastasis. Front Oncol 11: 656851, 2021.
10. Lu J: The Warburg metabolism fuels tumor metastasis. Cancer Metastasis Rev 38: 157-164, 2019.
11. Jiang B: Aerobic glycolysis and high level of lactate in cancer metabolism and microenvironment. Genes Dis 4: 25-27, 2017.
12. Contreras-Baeza Y, Sandoval PY, Alarcon R, Galaz A, Cortés-Molina F, Alegría K, Baeza-Lehnert F, Arce-Molina R, Guequén A, Flores CA, *et al*: Monocarboxylate transporter 4 (MCT4) is a high affinity transporter capable of exporting lactate in high-lactate microenvironments. J Biol Chem 294: 20135-20147, 2019.
13. Kong SC, Nohr-Nielsen A, Zeeberg K, Reshkin SJ, Hoffmann EK, Novak I and Pedersen SF: Monocarboxylate transporters MCT1 and MCT4 regulate migration and invasion of pancreatic ductal adenocarcinoma cells. Pancreas 45: 1036-1047, 2016.
14. Pinheiro C, Reis RM, Ricardo S, Longatto-Filho A, Schmitt F and Baltazar F: Expression of monocarboxylate transporters 1, 2, and 4 in human tumours and their association with CD147 and CD44. J Biomed Biotechnol 2010: 427694, 2010.
15. Choi JW, Kim Y, Lee JH and Kim YS: Prognostic significance of lactate/proton symporters MCT1, MCT4, and their chaperone CD147 expressions in urothelial carcinoma of the bladder. Urology 84: 245 e249-215, 2014.
16. Zhu J, Wu YN, Zhang W, Zhang XM, Ding X, Li HQ, Geng M, Xie ZQ and Wu HM: Monocarboxylate transporter 4 facilitates cell proliferation and migration and is associated with poor prognosis in oral squamous cell carcinoma patients. PLoS One 9: e87904, 2014.
17. Dong S, Zheng L and Jiang T: Loss of Lactate/Proton monocarboxylate transporter 4 induces ferroptosis via the AMPK/ACC pathway and inhibition of autophagy on human bladder cancer 5637 cell line. J Oncol 2023: 2830306, 2023.
18. Izumi H, Takahashi M, Uramoto H, Nakayama Y, Oyama T, Wang KY, Sasaguri Y, Nishizawa S and Kohno K: Monocarboxylate transporters 1 and 4 are involved in the invasion activity of human lung cancer cells. Cancer Sci 102: 1007-1013, 2011.
19. Gao HJ, Zhao MC, Zhang YJ, Zhou DS, Xu L, Li GB, Chen MS and Liu J: Monocarboxylate transporter 4 predicts poor prognosis in hepatocellular carcinoma and is associated with cell proliferation and migration. J Cancer Res Clin Oncol 141: 1151-1162, 2015.
20. Kong S, Nøhr-Nielsen A, Zeeberg K, Reshkin SJ, Hoffmann EK, Novak I and Pedersen SF: Monocarboxylate transporters MCT1 and MCT4 regulate migration and invasion of pancreatic ductal adenocarcinoma cells. Pancreas 45: 1036-1047, 2016.
21. Sun Q, Hu LL and Fu Q: MCT4 promotes cell proliferation and invasion of castration-resistant prostate cancer PC-3 cell line. EXCLI J 18: 187-194, 2019.
22. Reuss AM, Groos D, Ghoochani A, Buchfelder M and Savaskan N: MCT4 promotes tumor malignancy in F98 glioma Cells. J Oncol 2021: 6655529, 2021.
23. Li Z, Wu Q, Sun S, Wu J, Li J, Zhang Y, Wang C, Yuan J and Sun S: Monocarboxylate transporters in breast cancer and adipose tissue are novel biomarkers and potential therapeutic targets. Biochem Biophys Res Commun 501: 962-967, 2018.
24. Li X, Zhou X, Liu Y, Fan J, Huo H, Yao J, Wang L and Ma N: Overexpression of monocarboxylate transporter 4 promotes the migration and invasion of non-carcinogenic L929 fibroblast cells. Oncol Lett 21: 44, 2021.
25. Hu D, Zheng Y, Ou X, Zhang L, Du X and Shi S: Integrated analysis of anti-tumor roles of BAP1 in osteosarcoma. Front Oncol 12: 973914, 2022.
26. Tang Y, Li M, Wang J, Pan Y and Wu FX: CytoNCA: A cytoscape plugin for centrality analysis and evaluation of protein interaction networks. Biosystems 127: 67-72, 2015.
27. Girnita A, Girnita L, del Prete F, Bartolazzi A, Larsson O and Axelson M: Cyclolignans as inhibitors of the insulin-like growth factor-1 receptor and malignant cell growth. Cancer Res 64: 236-242, 2004.
28. Bieghs L, Lub S, Fostier K, Maes K, Van Valckenborgh E, Menu E, Johnsen HE, Overgaard MT, Larsson O, Axelson M, *et al*: The IGF-1 receptor inhibitor picropodophyllin potentiates the anti-myeloma activity of a BH3-mimetic. Oncotarget 5: 11193-11208, 2014.
29. Kong YL, Shen Y, Ni J, Shao DC, Miao NJ, Xu JL, Zhou L, Xue H, Zhang W, Wang XX and Lu LM: Insulin deficiency induces rat renal mesangial cell dysfunction via activation of IGF-1/IGF-1R pathway. Acta Pharmacol Sin 37: 217-227, 2016.
30. Sherk AB, Frigo DE, Schnackenberg CG, Bray JD, Laping NJ, Trizna W, Hammond M, Patterson JR, Thompson SK, Kazmin D, *et al*: Development of a small-molecule serum- and glucocorticoid-regulated kinase-1 antagonist and its evaluation as a prostate cancer therapeutic. Cancer Res 68: 7475-7483, 2008.
31. Mansley MK and Wilson SM: Effects of nominally selective inhibitors of the kinases PI3K, SGK1 and PKB on the insulin-dependent control of epithelial Na+ absorption. Br J Pharmacol 161: 571-588., 2010.
32. Harshitha R and Arunraj DR: Real-time quantitative PCR: A tool for absolute and relative quantification. Biochem Mol Biol Educ 49: 800-812, 2021.
33. Rodriguez LG, Wu X and Guan JL: Wound-healing assay. Methods Mol Biol 294: 23-29, 2005.

34. Li Q, Xu L, Li Y, Yang R, Qiao Q, Wang Y, Wang L, Guo Y and Guo C: P2RY14 is a potential biomarker of tumor microenvironment immunomodulation and favorable prognosis in patients with head and neck cancer. Front Genet 12: 670746, 2021.

35. Cho J, Yusuf R, Kook S, Attar E, Lee D, Park B, Cheng T, Scadden DT and Lee BC: Purinergic P2Y(1)(4) receptor modulates stress-induced hematopoietic stem/progenitor cell senescence. J Clin Invest 124: 3159-3171, 2014.

36. Xu T, Xu S, Yao Y, Chen X, Zhang Q, Zhao X, Wang X, Zhu J, Liu N, Zhang J, et al: P2RY14 downregulation in lung adenocarcinoma: A potential therapeutic target associated with immune infiltration. J Thorac Dis 14: 515-535, 2022.

37. Meng L, He X, Hong Q, Qiao B, Zhang X, Wu B, Zhang X, Wei Y, Li J, Ye Z and Xiao Y: CCR4, CCR8, and P2RY14 as prognostic factors in head and neck squamous cell carcinoma are involved in the remodeling of the tumor microenvironment. Front Oncol 11: 618187, 2021.

38. Wang H, Wang X, Xu L, Zhang J and Cao H: High expression levels of pyrimidine metabolic rate-limiting enzymes are adverse prognostic factors in lung adenocarcinoma: A study based on the cancer genome atlas and gene expression omnibus datasets. Purinergic Signal 16: 347-366, 2020.

39. Shah K, Moharram SA and Kazi JU: Acute leukemia cells resistant to PI3K/mTOR inhibition display upregulation of P2RY14 expression. Clin Epigenetics 10: 83, 2018.

40. Woods LT, Forti KM, Shanbhag VC, Camden JM and Weisman GA: P2Y receptors for extracellular nucleotides: Contributions to cancer progression and therapeutic implications. Biochem Pharmacol 187: 114406, 2021.

41. Cohen P: Serum insulin-like growth factor-i levels and prostate cancer risk-interpreting the evidence. J Natl Cancer Inst 90: 876-879, 1998.

42. Wang X, Zhu Q, Lin Y, Wu L, Wu X, Wang K, He Q, Xu C, Wan X and Wang X: Crosstalk between TEMs and endothelial cells modulates angiogenesis and metastasis via IGF1-IGF1R signalling in epithelial ovarian cancer. Br J Cancer 117: 1371-1382, 2017.

43. Peyrat J, Bonneterre J, Vennin P, Jammes H, Beuscart R, Hecquet B, Djiane J, Lefebvre J and Demaille A: Insulin-like growth factor 1 receptors (IGF1-R) and IGF1 in human breast tumors. J Steroid Biochem Mol Biol 37: 823-827, 1990.

44. Liu Y, Nelson MV, Bailey C, Zhang P, Zheng P, Dome JS, Liu Y and Wang Y: Targeting the HIF-1α-IGFBP2 axis therapeutically reduces IGF1-AKT signaling and blocks the growth and metastasis of relapsed anaplastic Wilms tumor. Oncogene 40: 4809-4819, 2021.

45. Yang L, Tan Z, Li Y, Zhang X, Wu Y, Xu B and Wang M: Insulin-like growth factor 1 promotes proliferation and invasion of papillary thyroid cancer through the STAT3 pathway. J Clin Lab Anal 34: e23531, 2020.

46. Chen ZL, Li XN, Ye CX, Chen HY and Wang ZJ: Elevated levels of circRUNX1 in colorectal cancer promote cell growth and metastasis via miR-145-5p/IGF1 signalling. Onco Targets Ther 13: 4035-4048, 2020.

47. Wang H, Tang C, Na M, Ma W, Jiang Z, Gu Y, Ma G, Ge H, Shen H and Lin Z: miR-422a inhibits glioma proliferation and invasion by targeting IGF1 and IGF1R. Oncol Res 25: 187-194, 2017.

48. Lu X, Song X, Hao X, Liu X, Zhang X, Yuan N, Ma H and Zhang Z: MiR-186-3p attenuates tumorigenesis of cervical cancer by targeting IGF1. World J Surg Oncol 19: 207, 2021.

49. Nagle AM, Levine KM, Tasdemir N, Scott JA, Burlbaugh K, Kehm J, Katz TA, Boone DN, Jacobsen BM, Atkinson JM, et al: Loss of E-cadherin enhances IGF1-IGF1R pathway activation and sensitizes breast cancers to anti-IGF1R/InsR inhibitors. Clin Cancer Res 24: 5165-5177, 2018.

50. Hirakawa T, Yashiro M, Doi Y, Kinoshita H, Morisaki T, Fukuoka T, Hasegawa T, Kimura K, Amano R and Hirakawa K: Pancreatic fibroblasts stimulate the motility of pancreatic cancer cells through IGF1/IGF1R signaling under hypoxia. PLoS One 11: e0159912, 2016.

51. Fürstenberger G and Senn HJ: Insulin-like growth factors and cancer. Lancet Oncol 3: 298-302, 2002.

52. Matà R, Palladino C, Nicolosi M, Lo Presti AR, Malaguarnera R, Ragusa M, Sciortino D, Morrione A, Maggiolini M, Vella V and Belfiore A: IGF-I induces upregulation of DDR1 collagen receptor in breast cancer cells by suppressing MIR-199a-5p through the PI3K/AKT pathway. Oncotarget 7: 7683-7700, 2016.

53. Zhou J, Chen G, Tang Y, Sinha RA, Wu Y, Yap CS, Wang G, Hu J, Xia X, Tan P, et al: Genetic and bioinformatic analyses of the expression and function of PI3K regulatory subunit PIK3R3 in an Asian patient gastric cancer library. BMC Med Genomics 5: 1-8, 2012.

54. Zhu Y, Zhao H, Rao M and Xu S: MicroRNA-365 inhibits proliferation, migration and invasion of glioma by targeting PIK3R3. Oncol Rep 37: 2185-2192, 2017.

55. Sun H and Feng X: MicroRNA-367 directly targets PIK3R3 to inhibit proliferation and invasion of oral carcinoma cells. Biosci Rep 40: BSR20193867, 2020.

56. Qi J, Wang WW, Chen W, Lu WY and Shang AQ: Mechanism of miR-137 regulating migration and invasion of melanoma cells by targeting PIK3R3 gene. J Cell Biochem 120: 8393-8400, 2018.

57. Bruhn MA, Pearson RB, Hannan RD and Sheppard KE: Second AKT: The rise of SGK in cancer signalling. Growth Factors 28: 394-408, 2010.

58. Sang Y, Kong P, Zhang S, Zhang L, Cao Y, Duan X, Sun T, Tao Z and Liu W: SGK1 in human cancer: Emerging roles and mechanisms. Front Oncol 10: 608722, 2020.

59. Liang X, Lan C, Jiao G, Fu W, Long X, An Y, Wang K, Zhou J, Chen T, Li Y, et al: Therapeutic inhibition of SGK1 suppresses colorectal cancer. Exp Mol Med 49: e399, 2017.

60. Greenawalt EJ, Edmonds MD, Jain N, Adams CM, Mitra R and Eischen CM: Targeting of SGK1 by miR-576-3p inhibits lung adenocarcinoma migration and invasion. Mol Cancer Res 17: 289-298, 2019.

61. Liu W, Wang X, Wang Y, Dai Y, Xie Y, Ping Y, Yin B, Yu P, Liu Z, Duan X, et al: SGK1 inhibition-induced autophagy impairs prostate cancer metastasis by reversing EMT. J Exp Clin Cancer Res 37: 73, 2018.

62. Zhu R, Yang G, Cao Z, Shen K, Zheng L, Xiao J, You L and Zhang T: The prospect of serum and glucocorticoid-inducible kinase 1 (SGK1) in cancer therapy: A rising star. Ther Adv Med Oncol 12: 1758835920940946, 2020.

63. Zhang Y, Shi G, Zhang H, Xiong Q, Cheng F, Wang H, Luo J, Zhang Y, Shi P, Xu J, et al: Dexamethasone enhances the lung metastasis of breast cancer via a PI3K-SGK1-CTGF pathway. Oncogene 40: 5367-5378, 2021.

64. Gallagher SM, Castorino JJ and Philp NJ: Interaction of monocarboxylate transporter 4 with beta1-integrin and its role in cell migration. Am J Physiol Cell Physiol 296: C414-C421, 2009.

65. Niu Z, Yang F, Li H, Wang J, Ni Q, Ma C, Zhu H, Chang H, Zhou X, Lu J and Gao H: MCT4 promotes hepatocellular carcinoma progression by upregulating TRAPPC5 gene. J Hepatocell Carcinoma 9: 289-300, 2022.

66. Ma J, Sawai H, Matsuo Y, Ochi N, Yasuda A, Takahashi H, Wakasugi T, Funahashi H, Sato M and Takeyama H: IGF-1 mediates PTEN suppression and enhances cell invasion and proliferation via activation of the IGF-1/PI3K/Akt signaling pathway in pancreatic cancer cells. J Surg Res 160: 90-101, 2010.

67. Cheng CJ and Huang CL: Activation of PI3-kinase stimulates endocytosis of ROMK via Akt1/SGK1-dependent phosphorylation of WNK1. J Am Soc Nephrol 22: 460-471, 2011.

68. Heinrich T, Sala-Hojman A, Ferretti R, Petersson C, Minguzzi S, Gondela A, Ramaswamy S, Bartosik A, Czauderna F, Crowley L, et al: Discovery of 5-2-[5-Chloro-2-(5-ethoxyquinoline-8-sulfonamido)phenyl]ethynyl-4-methoxypyridine-2-carboxylic acid, a highly selective in vivo useable chemical probe to dissect MCT4 biology. J Med Chem 64: 11904-11933, 2021.

69. Qiang YW, Yao L, Tosato G and Rudikoff S: Insulin-like growth factor I induces migration and invasion of human multiple myeloma cells. Blood 103: 301-308, 2004.

70. Seo SH, Hwang SY, Hwang S, Han S, Park H, Lee YS, Rho SB and Kwon Y: Hypoxia-induced ELF3 promotes tumor angiogenesis through IGF1/IGF1R. EMBO Rep 23: e52977, 2022.

71. Fukuda R, Hirota K, Fan F, Jung YD, Ellis LM and Semenza GL: Insulin-like growth factor 1 induces hypoxia-inducible factor 1-mediated vascular endothelial growth factor expression, which is dependent on MAP kinase and phosphatidylinositol 3-kinase signaling in colon cancer cells. J Biol Chem 277: 38205-38211, 2002.

72. Jena B, Das C, Banerjee I, Bharadwaj D, Majumder R, Das S, Biswas A, Kundu M, Roy PK, Kundu CN and Mandal M: TGF-β1 induced autophagy in cancer associated fibroblasts during hypoxia contributes EMT and glycolysis via MCT4 upregulation. Exp Cell Res 417: 113195, 2022.